

# Chapter 13

## Shaft Couplings

A shaft coupling is, in the broadest sense, a mechanical device transmitting rotational motion from a shaft 1 to another shaft 2. In addition, a shaft coupling may serve the purpose of keeping one shaft in position relative to the other. Example: If both shafts are mounted in bearings in a common frame, a pair of gears having the transmission ratio one (spur gears, bevel gears or hypoid gears depending on the relative location of the shafts) is a shaft coupling transmitting rotational motion in such a way that  $\omega_1 = \text{const}$  in shaft 1 causes  $\omega_2 \equiv \omega_1 = \text{const}$  in shaft 2. If both shafts are mounted in parallel and sufficiently close together, an Oldham coupling is serving the same purpose. The Oldham coupling is functioning properly even in the case when the distance between the shafts is changing during operation. Neither gears nor Oldham couplings serve the purpose of keeping one shaft in position relative to the other. Another example: Only shaft 1 is mounted in fixed bearings. Shaft 2 is required to intersect shaft 1 at a given point  $O$  whereas its direction is free to change. Bevel gears are not applicable in this case. A common Hooke's joint (also called universal joint) is a possible shaft coupling. Its cross-shaped central body serves the purpose of keeping the shafts intersecting at  $O$ . In addition, rotational motion is transmitted from shaft 1 to shaft 2. However, as will be seen in the following section,  $\omega_1 = \text{const}$  in shaft 1 does not cause  $\omega_2 \equiv \omega_1 = \text{const}$  in shaft 2. Shaft couplings allowing changes of relative position while maintaining the identity  $\omega_2 \equiv \omega_1$  are called homokinetic. The general theory of homokinetic couplings is the subject of Sect. 13.4. The engineering importance and a simple example were explained in Sect. 4.2.6.

### 13.1 Hooke's Joint

In the plane of Fig. 13.1 two shafts 1 and 2 are mounted in bearings such that the shaft axes intersect at point 0 under a constant angle  $\alpha$ . The shafts are coupled by a Hooke's joint. Its essential element is a cross-shaped central body. Each shaft is connected to this body by a revolute joint the axis of which is normal to the shaft. On the central body the two joint axes intersect orthogonally at 0. In the figure the system is shown in a position in which one axis of the central body is in the plane of the drawing, while the other axis is perpendicular to it. The central body and the two revolute joints together constitute Hooke's joint. The angle  $\alpha$  is a free parameter which in Fig. 13.1 is prescribed by the other two revolute joints connecting the shafts to a frame. The entire system composed of frame, shafts, central body and of four revolute joints represents a spherical four-bar with center 0. From Chap. 4 it is known that the degree of freedom is one. Thus, Hooke's joint transmits a rotation from shaft 1 to shaft 2. Let  $\varphi_1$  and  $\varphi_2$  be the angles of rotation of shaft 1 and of shaft 2, respectively, relative to the frame. They are related by a constraint equation  $f(\varphi_1, \varphi_2) = 0$ . In what follows, this equation is formulated. Subsequently, various other kinematical relationships are derived from this equation.

In Fig. 13.1  $\underline{e}^1$  and  $\underline{e}^2$  are two reference bases fixed on the frame. Their common basis vectors  $\underline{e}_3^1 = \underline{e}_3^2$  are normal to the plane of the two shafts, and  $\underline{e}_1^1$  and  $\underline{e}_1^2$  are directed along the respective shaft axes. The bases are related by the constant transformation matrix

$$A^{12} = \begin{bmatrix} \cos \alpha & -\sin \alpha & 0 \\ \sin \alpha & \cos \alpha & 0 \\ 0 & 0 & 1 \end{bmatrix}. \tag{13.1}$$

Let  $\underline{n}_1$  and  $\underline{n}_2$  be unit vectors fixed on the central body along the joint axes. In the position shown in Fig. 13.1  $\underline{n}_1 = \underline{e}_2^1$ . Let this be the position  $\varphi_1 = 0$  of shaft 1 and the position  $\varphi_2 = -\pi/2$  of shaft 2. This means that  $\varphi_2 = 0$  is the position when  $\underline{n}_2 = \underline{e}_2^2$ . In a position  $\varphi_1$  (arbitrary)  $\underline{n}_1$  has

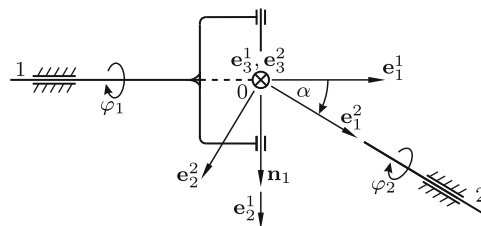


Fig. 13.1 Hooke's joint with frame-fixed bases  $\underline{e}^1, \underline{e}^2$  in position  $\varphi_1 = 0, \varphi_2 = -\pi/2$

in basis  $\mathbf{e}^1$  the coordinate matrix  $\underline{n}_1^1 = [0 \quad \cos \varphi_1 \quad \sin \varphi_1]^T$ . Similarly, in a position  $\varphi_2$  (arbitrary)  $\mathbf{n}_2$  has in  $\mathbf{e}^2$  the coordinate matrix

$$\underline{n}_2^2 = [0 \quad \cos \varphi_2 \quad \sin \varphi_2]^T. \tag{13.2}$$

Transformation yields the coordinate matrix  $\underline{n}_2^1 = \underline{A}^{12} \underline{n}_2^2$  in basis  $\mathbf{e}^1$ . The coordinate matrices  $\underline{n}_1^1$  and  $\underline{n}_2^1$  determine the coordinate matrix  $\underline{n}_3^1 = \tilde{n}_1^1 \underline{n}_2^1$  of the vector  $\mathbf{n}_3 = \mathbf{n}_1 \times \mathbf{n}_2$ . The three coordinate matrices are

$$\begin{aligned} \underline{n}_1^1 = & \quad \underline{n}_2^1 = & \quad \underline{n}_3^1 = \\ \begin{bmatrix} 0 \\ \cos \varphi_1 \\ \sin \varphi_1 \end{bmatrix}, & \begin{bmatrix} -\sin \alpha \cos \varphi_2 \\ \cos \alpha \cos \varphi_2 \\ \sin \varphi_2 \end{bmatrix}, & \begin{bmatrix} -\cos \alpha \sin \varphi_1 \cos \varphi_2 + \cos \varphi_1 \sin \varphi_2 \\ -\sin \alpha \sin \varphi_1 \cos \varphi_2 \\ \sin \alpha \cos \varphi_1 \cos \varphi_2 \end{bmatrix}. \end{aligned} \tag{13.3}$$

From the first two matrices the desired relationship  $f(\varphi_1, \varphi_2) = 0$  is obtained. Orthogonality of the vectors  $\mathbf{n}_1$  and  $\mathbf{n}_2$  requires that  $\mathbf{n}_1 \cdot \mathbf{n}_2 = 0$ . This is the equation  $f(\varphi_1, \varphi_2) = \cos \varphi_1 \cos \alpha \cos \varphi_2 + \sin \varphi_1 \sin \varphi_2 = 0$  or

$$\tan \varphi_2 \tan \varphi_1 = -\cos \alpha. \tag{13.4}$$

This relationship was first published in 1824 by Jean Victor Poncelét (1788-1867) (see also Poncelét [15]). The output angle  $\varphi_2$  is an odd,  $\pi$ -periodic function of the input angle  $\varphi_1$ . It is independent of the sign of  $\alpha$ . In view of Fig. 13.1 this had to be expected. The equation yields the expressions

$$\left. \begin{aligned} \cos \varphi_2 &= \frac{1}{\sqrt{1 + \tan^2 \varphi_2}} = \frac{\sin \varphi_1}{\sqrt{1 - \sin^2 \alpha \cos^2 \varphi_1}}, \\ \sin \varphi_2 &= \frac{-\cos \alpha \cos \varphi_1}{\sqrt{1 - \sin^2 \alpha \cos^2 \varphi_1}}. \end{aligned} \right\} \tag{13.5}$$

Differentiation of (13.4) with respect to time results in the equation  $(\dot{\varphi}_2 / \cos^2 \varphi_2) \tan \varphi_1 + (\dot{\varphi}_1 / \cos^2 \varphi_1) \tan \varphi_2 = 0$ . This yields for the angular velocity ratio the expression

$$\frac{\dot{\varphi}_2}{\dot{\varphi}_1} = -\frac{\sin \varphi_2 \cos \varphi_2}{\sin \varphi_1 \cos \varphi_1}. \tag{13.6}$$

Elimination of  $\varphi_2$  by means of (13.5) leads to the final formula

$$\frac{\dot{\varphi}_2}{\dot{\varphi}_1} = \frac{\cos \alpha}{1 - \sin^2 \alpha \cos^2 \varphi_1}. \tag{13.7}$$

This is an even  $\pi$ -periodic function of  $\varphi_1$ . In the case  $\dot{\varphi}_1 = \text{const}$ , the angular velocity  $\dot{\varphi}_2$  is oscillating  $\pi$ -periodically between the extremal values  $\dot{\varphi}_1 \cos \alpha$  and  $\dot{\varphi}_1 / \cos \alpha$ .

One more differentiation with respect to time yields for the angular acceleration  $\ddot{\varphi}_2$  the expression (valid for  $\dot{\varphi}_1 = \text{const}$ )

$$\ddot{\varphi}_2 = -\dot{\varphi}_1^2 \frac{\sin^2 \alpha \cos \alpha \sin 2\varphi_1}{(1 - \sin^2 \alpha \cos^2 \varphi_1)^2}, \quad \ddot{\varphi}_2 \approx -\dot{\varphi}_1^2 \alpha^2 \sin 2\varphi_1 \quad (\alpha \ll 1). \quad (13.8)$$

The difference  $\chi(\varphi_1) = \varphi_2 - \varphi_1 + \pi/2$  is an odd  $\pi$ -periodic function of  $\varphi_1$  (note that  $\varphi_2 = -\pi/2$  when  $\varphi_1 = 0$ ). Its maxima and minima of equal absolute value occur in positions when  $\dot{\varphi}_2 = \dot{\varphi}_1$ . According to (13.7) this is the case when  $\cos^2 \varphi_1 = 1/(1 + \cos \alpha)$ . From this it follows that  $\sin^2 \varphi_1 = \cos \alpha / (1 + \cos \alpha)$  and  $\tan \varphi_1 = \sqrt{\cos \alpha}$ . Furthermore, according to (13.4),  $\tan \varphi_2 = -\sqrt{\cos \alpha}$ . This yields for the maximum of  $\chi$  the formula

$$\begin{aligned} \tan \left( \chi_{\max} - \frac{\pi}{2} \right) &= -\cot \chi_{\max} = \tan(\varphi_2 - \varphi_1) \\ &= \frac{\tan \varphi_2 - \tan \varphi_1}{1 - \tan \varphi_2 \tan \varphi_1} = \frac{-2\sqrt{\cos \alpha}}{1 - \cos \alpha}. \end{aligned} \quad (13.9)$$

Hence

$$\chi_{\max} = \tan^{-1} \frac{1 - \cos \alpha}{2\sqrt{\cos \alpha}}. \quad (13.10)$$

**Example:**  $\chi_{\max} \approx 4.1^\circ$  at  $\varphi_1 \approx 42.9^\circ$  for  $\alpha = 30^\circ$ . The Taylor formula for small angles  $\alpha$  is  $\chi_{\max} \approx \alpha^2/4$ . End of example.

### 13.1.1 Polhode and Herpolhode Cones of the Central Cross

The cross-shaped central body is executing a periodic motion about a fixed point. For this reason, both the polhode cone and the herpolhode cone are closed cones. In what follows, these cones are determined<sup>1</sup>. Let  $\dot{\psi}_1 \mathbf{n}_1$  and  $\dot{\psi}_2 \mathbf{n}_2$  be the angular velocities of the cross relative to the two shafts so that the angular velocity  $\boldsymbol{\omega}$  of the cross relative to the frame has the alternative forms

$$\boldsymbol{\omega} = \dot{\varphi}_1 \mathbf{e}_1^1 + \dot{\psi}_1 \mathbf{n}_1 = \dot{\varphi}_2 \mathbf{e}_1^2 + \dot{\psi}_2 \mathbf{n}_2. \quad (13.11)$$

In the reference basis with basis vectors  $\mathbf{n}_1, \mathbf{n}_2, \mathbf{n}_3 = \mathbf{n}_1 \times \mathbf{n}_2$  fixed on the cross  $\boldsymbol{\omega}$  has the coordinates

$$\omega_1 = \dot{\psi}_1 = \dot{\varphi}_2 \mathbf{e}_1^2 \cdot \mathbf{n}_1, \quad \omega_2 = \dot{\psi}_2 = \dot{\varphi}_1 \mathbf{e}_1^1 \cdot \mathbf{n}_2, \quad \omega_3 = \dot{\varphi}_1 \mathbf{e}_1^1 \cdot \mathbf{n}_3. \quad (13.12)$$

<sup>1</sup> In Wittenburg/Roberson [18] the cones are determined for a Hooke's joint with a nonorthogonal central cross

The scalar products are read from (13.2) and (13.3). For  $\cos \varphi_2$ ,  $\sin \varphi_2$  and  $\dot{\varphi}_2$  the expressions (13.5) and (13.7) are substituted. This results in

$$\left. \begin{aligned} \omega_1 = \dot{\psi}_1 = \dot{\varphi}_1 \frac{\sin \alpha \cos \alpha \cos \varphi_1}{1 - \sin^2 \alpha \cos^2 \varphi_1}, \quad \omega_2 = -\dot{\varphi}_1 \frac{\sin \alpha \sin \varphi_1}{\sqrt{1 - \sin^2 \alpha \cos^2 \varphi_1}}, \\ \omega_3 = \dot{\varphi}_1 \frac{-\cos \alpha}{\sqrt{1 - \sin^2 \alpha \cos^2 \varphi_1}}. \end{aligned} \right\} \quad (13.13)$$

These equations are parameter equations of the polhode cone (the moving cone) with  $\varphi_1$  as parameter. The cone is best portrayed by its curve of intersection with a plane parallel to the  $\mathbf{n}_1, \mathbf{n}_2$ -plane. This curve has the parameter equations

$$x(\varphi_1) = \frac{\omega_1}{\omega_3} = \frac{-\sin \alpha \cos \varphi_1}{\sqrt{1 - \sin^2 \alpha \cos^2 \varphi_1}}, \quad y(\varphi_1) = \frac{\omega_2}{\omega_3} = \tan \alpha \sin \varphi_1. \quad (13.14)$$

Squaring both equations leads to expressions for  $\cos^2 \varphi_1$  and for  $\sin^2 \varphi_1$ . Their sum equals one. This is the parameter-free equation

$$x^2 + x^2 y^2 + y^2 = \tan^2 \alpha. \quad (13.15)$$

In Fig. 13.2 curves are shown for various angles  $\alpha$ . The ellipse is explained later. An investigation of the curvature shows that the transition from convex to nonconvex curves occurs at  $\alpha = 60^\circ$ . The smaller  $\alpha$  the better is the approximation of a circle of radius  $\alpha$ . In joints used in engineering angles up to approximately  $\alpha = 35^\circ$  are realizable. At the points of symmetry of the curve marked by  $|x| = |y|$  (13.15) yields  $y^2 = 1/\cos \alpha - 1$ . Equation (13.14) yields for the associated angle  $\varphi_1$  the expression  $\sin \varphi_1 = \sqrt{\cos \alpha / (1 + \cos \alpha)}$ . This is the angle associated with the maximum difference  $\chi_{\max}$ .

The herpolhode cone (the fixed cone) is determined by the coordinates of  $\boldsymbol{\omega}$  in basis  $\underline{\mathbf{e}}^1$ . Let these coordinates be denoted  $\Omega_1, \Omega_2, \Omega_3$ . Equation (13.11) in combination with (13.3) and with  $\dot{\psi}_1$  from (13.13) results in

$$\left. \begin{aligned} \Omega_1 = \dot{\varphi}_1, \quad \Omega_2 = \dot{\psi}_1 \mathbf{n}_1 \cdot \mathbf{e}_2^1 = \dot{\varphi}_1 \frac{\sin \alpha \cos \alpha \cos^2 \varphi_1}{1 - \sin^2 \alpha \cos^2 \varphi_1}, \\ \Omega_3 = \dot{\psi}_1 \mathbf{n}_1 \cdot \mathbf{e}_3^1 = \dot{\varphi}_1 \frac{\sin \alpha \cos \alpha \sin \varphi_1 \cos \varphi_1}{1 - \sin^2 \alpha \cos^2 \varphi_1}. \end{aligned} \right\} \quad (13.16)$$

This yields the ratios

$$\left. \begin{aligned} X(\varphi_1) = \frac{\Omega_2}{\Omega_1} = \frac{\sin \alpha \cos \alpha \cos^2 \varphi_1}{1 - \sin^2 \alpha \cos^2 \varphi_1}, \\ Y(\varphi_1) = \frac{\Omega_3}{\Omega_1} = \frac{\sin \alpha \cos \alpha \sin \varphi_1 \cos \varphi_1}{1 - \sin^2 \alpha \cos^2 \varphi_1}. \end{aligned} \right\} \quad (13.17)$$

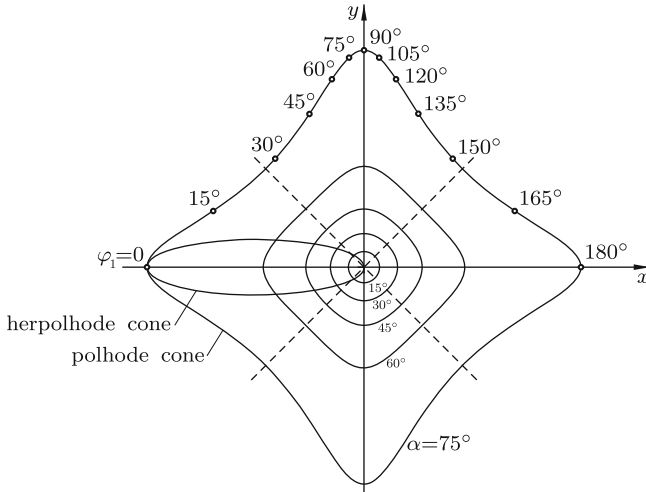


**Fig. 13.2** Intersection curves of polhode cones of the cross-shaped central body with a plane parallel to the  $\mathbf{n}_1, \mathbf{n}_2$ -plane for Hooke's joints with various angles  $\alpha$ . The ellipse represents the herpolhode cone associated with  $\alpha = 75^\circ$  in the position  $\varphi_1 = 0$

They are parameter equations of the intersection curve of the herpolhode cone with a plane normal to the shaft axis  $\mathbf{e}_1^1$ . The parameter  $\varphi_1$  is eliminated by calculating  $\tan \varphi_1 = Y/X$  and hence  $\cos^2 \varphi_1 = X^2/(X^2 + Y^2)$ . This expression is substituted back into the equation for  $X(\varphi_1)$ . The result is the ellipse

$$\left(\frac{X - \frac{1}{2} \tan \alpha}{\frac{1}{2} \tan \alpha}\right)^2 + \left(\frac{Y}{\frac{1}{2} \sin \alpha}\right)^2 = 1. \tag{13.18}$$

Figure 13.3 shows the location of the herpolhode cone and of this ellipse relative to the two shafts. Both shaft axes are generators of the cone. The projection of the ellipse along the axis of shaft 2 is a circle. In the position  $\varphi_1 = 0$  the planes of intersection of the cones coincide, and the common generator  $\omega$  lies in the shaft axis 2. In Fig. 13.2 the ellipse associated with  $\alpha = 75^\circ$  is shown in this position. For arbitrary  $\alpha$  and in every position  $\varphi_1$  the fixed cone lies entirely inside the moving cone so that rolling of one cone on the other is possible without collision. Per revolution of shaft 1 the vector

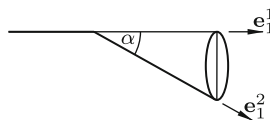


**Fig. 13.3** Herpolhode cone with elliptic cross section between the shaft axes

$\omega$  is sweeping out the fixed cone twice and the moving cone once. This means that the moving cone is rolling around the fixed cone twice per revolution of shaft 1.

The cones are known from Sect. 10.1. The motion studied there is the inverse of the motion of the central cross. The moving cone of one motion is the fixed cone of the other and vice versa (compare (13.15) and (13.18) with (10.19)).

In preparation for Sect. 13.2.1 the angle of rotation  $\psi_1$  of the cross relative to shaft 1 is determined as function of  $\varphi_1$ . Arbitrarily,  $\psi_1 = 0$  is associated with  $\varphi_1 = 0$ . From (13.12) and (13.13) it follows that

$$\frac{d\psi_1}{d\varphi_1} = \frac{\sin \alpha \cos \alpha \cos \varphi_1}{1 - \sin^2 \alpha \cos^2 \varphi_1}. \tag{13.19}$$

With the new variable  $z = \tan \varphi_1/2$  and with the constant  $k^2 = (1 - \sin \alpha)/(1 + \sin \alpha)$  this takes the form

$$\begin{aligned} \psi_1 &= 2 \tan \alpha \int \frac{1 - z^2}{(1 + k^2 z^2)(1 + z^2/k^2)} dz \\ &= \frac{2 \tan \alpha}{k^2 - 1} \left[ k^2 \int \frac{dz}{1 + k^2 z^2} - \int \frac{dz}{1 + z^2/k^2} \right] \\ &= \tan^{-1}(z/k) - \tan^{-1}(kz) = \tan^{-1}(\tan \alpha \sin \varphi_1). \end{aligned} \tag{13.20}$$

Hence

$$\tan \psi_1 = \tan \alpha \sin \varphi_1. \tag{13.21}$$

This equation is the second Eq.(10.10).

### 13.2 Fenyi's Joint

Figure 13.4 is the exploded view of a shaft coupling brought to the author's attention by Fenyi<sup>2</sup>. The coupled shafts 1 and 2 are skew. They are mounted in frame-fixed bearings not shown in the figure. Let  $\hat{e}_1^1$  and  $\hat{e}_2^2$  be dual unit vectors along the shaft axes, and let, furthermore,  $\hat{\alpha} = \alpha + \varepsilon \ell$  be the constant dual screw angle displacing  $\hat{e}_1^1$  into the position  $\hat{e}_2^2$ . The projected angle  $\alpha$  and the length  $\ell$  of the common perpendicular of the two shaft axes are the only parameters of the joint. To each shaft and at right angles to the shaft two collinear trunnions are rigidly attached. These trunnions are moving in bearings of the central ring-shaped body. The axes of these bearings intersect at a right angle at M. In the assembled state the ring transmits the rotational motion of shaft 1 to shaft 2. Relative to each pair

---

<sup>2</sup> Stanislo Fenyi, Forschungszentrum Karlsruhe

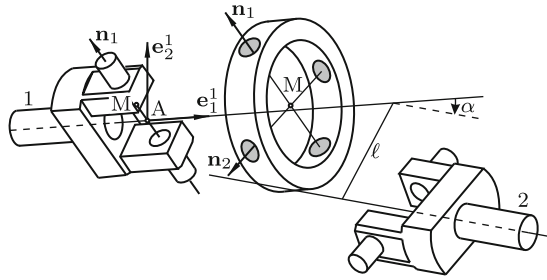


**Fig. 13.4** Exploded view of Fenyi's joint

of trunnions the ring executes a screw motion. It is assumed that shaft 1 is in pure rotation relative to the frame (angle of rotation  $\varphi_1$ ). In order to function properly the bearings of shaft 2 must allow shaft 2 to execute a screw motion composed of a rotation  $\varphi_2$  and a translation  $z$ . In the special case  $\alpha = 0$ , the joint is the Oldham coupling shown in Fig. 15.6. In the special case  $\ell = 0$ , the joint is Hooke's joint shown in Fig. 13.1, and all screw displacements are pure rotations.

The following kinematics investigation is based on the principle of transference. The rotational part of the problem is identical with that of a Hooke's joint with parameter  $\alpha$ . The principle of transference is applied to Eq.(13.4):

$$\tan \varphi_2 \tan \varphi_1 = -\cos \alpha . \tag{13.22}$$

The angle  $\alpha$  is replaced by  $\hat{\alpha} = \alpha + \varepsilon \ell$ , and the angle  $\varphi_2$  is replaced by  $\hat{\varphi}_2 = \varphi_2 + \varepsilon z$ . The angle  $\varphi_1$  is not effected because shaft 1 is, by assumption, in pure rotation. Thus, the dual form of (13.22) is  $\tan \hat{\varphi}_2 \tan \varphi_1 = -\cos \hat{\alpha}$ . This is the equation (see (3.31))

$$\left( \tan \varphi_2 + \varepsilon \frac{z}{\cos^2 \varphi_2} \right) \tan \varphi_1 = -(\cos \alpha - \varepsilon \ell \sin \alpha) . \tag{13.23}$$

The primary part of this equation is Eq.(13.22). The dual part is  $(z/\cos^2 \varphi_2) \tan \varphi_1 = \ell \sin \alpha$ . Writing  $1/\cos^2 \varphi_2 = 1 + \tan^2 \varphi_2$  and using (13.22) this yields for the translatory displacement of shaft 2 the expression

$$z = \ell \frac{\sin \alpha \sin \varphi_1 \cos \varphi_1}{1 - \sin^2 \alpha \cos^2 \varphi_1} . \tag{13.24}$$

This is an odd,  $\pi$ -periodic function of  $\varphi_1$ . Its maxima and minima of equal absolute value occur when  $dz/d\varphi_1 = 0$ . This equation leads to  $\cos^2 \varphi_1 = 1/(1 + \cos^2 \alpha)$ ,  $\sin^2 \varphi_1 = \cos^2 \alpha/(1 + \cos^2 \alpha)$  and  $\sin \varphi_1 \cos \varphi_1 = \cos \alpha/(1 + \cos^2 \alpha)$ . When this is substituted into (13.24), the maximum range of the translatory displacement of shaft 2 is found to be

$$z_{\max} - z_{\min} = 2z_{\max} = \ell \tan \alpha . \tag{13.25}$$

### 13.2.1 Raccording Axodes of the Central Ring

The central ring is executing a periodic spatial motion without a fixed point. The periodically moving instantaneous screw axis is the generator of two closed raccording axodes. In what follows, parameter equations with  $\varphi_1$  as parameter are developed for these axodes. On the frame the basis  $\underline{\mathbf{e}}^1$  known from Fig. 13.1 is fixed. Its origin A is the point where the axis of shaft 1 intersects the first axis of the ring. On the ring the basis  $\underline{\mathbf{n}}$  with basis vectors  $\mathbf{n}_1, \mathbf{n}_2, \mathbf{n}_3$  known from Fig. 13.1 is defined. It has its origin at the point of intersection M of the two ring axes. By writing the vector from A to M in the form  $z_1 \mathbf{n}_1$  the coordinate  $z_1 = z_1(\varphi_1)$  is defined. Let  $\mathbf{u}(\varphi_1)$  be the perpendicular from A onto the instantaneous screw axis (ISA) of the ring, and let, furthermore,  $\boldsymbol{\omega}(\varphi_1)$  be the angular velocity of the ring relative to the frame. With a dimensionless parameter  $\lambda$  the vectors from A and from M to an arbitrary point P( $\lambda$ ) on the ISA are

$$\left. \begin{aligned} \mathbf{r}_{\text{AP}}(\varphi_1, \lambda) &= \mathbf{u}(\varphi_1) + \frac{\lambda \ell}{\varphi_1} \boldsymbol{\omega}(\varphi_1) , \\ \mathbf{r}_{\text{MP}}(\varphi_1, \lambda) &= \mathbf{u}(\varphi_1) + \frac{\lambda \ell}{\varphi_1} \boldsymbol{\omega}(\varphi_1) - z_1(\varphi_1) \mathbf{n}_1 . \end{aligned} \right\} \tag{13.26}$$

The coordinates of  $\mathbf{r}_{\text{AP}}$  in basis  $\underline{\mathbf{e}}^1$  and the coordinates of  $\mathbf{r}_{\text{MP}}$  in basis  $\underline{\mathbf{n}}$  are the desired parameter equations of the fixed axode and of the moving axode, respectively. With increasing  $|\lambda|$  the equations of the axodes approach asymptotically those of the herpolhode cone and of the polhode cone, respectively, of the cross-shaped central body in Hooke's joint (see Figs. 13.2 and 13.3).

The perpendicular  $\mathbf{u}$  from A onto the ISA is, according to (9.23),

$$\mathbf{u} = \frac{\boldsymbol{\omega} \times \mathbf{v}_A}{\boldsymbol{\omega}^2} \tag{13.27}$$

with  $\mathbf{v}_A$  being the velocity of the ring-fixed point coinciding with A. This velocity is  $\mathbf{v}_A = \dot{z}_1 \mathbf{n}_1$ . Expressions for  $z_1$  and for  $\dot{z}_1$  are obtained by transferring Eq.(13.21) into dual form:  $\tan(\psi_1 + \varepsilon z_1) = \tan(\alpha + \varepsilon \ell) \sin \varphi_1$ . Its dual part is the expression for  $z_1$  given below. Differentiation<sup>3</sup> yields  $\dot{z}_1$ . With the abbreviations  $C = \cos \alpha$ ,  $S = \sin \alpha$ ,  $c = \cos \varphi_1$ ,  $s = \sin \varphi_1$  the expressions are

---

<sup>3</sup>  $\dot{z}_1$  is also the dual part of the dualized expression for  $\dot{\psi}_1$  given in the first Eq.(13.29)

$$z_1 = \ell \frac{s}{1 - S^2 c^2}, \quad \dot{z}_1 = \dot{\varphi}_1 \ell \frac{c(C^2 - S^2 s^2)}{(1 - S^2 c^2)^2}. \tag{13.28}$$

The angular velocity  $\boldsymbol{\omega}$  of the ring is identical with the angular velocity of the cross-shaped body in Hooke’s joint. From (13.11), (13.12) and (13.13) the following expressions are copied:

$$\left. \begin{aligned} \psi_1 &= \dot{\varphi}_1 \frac{SCc}{1 - S^2 c^2}, & \boldsymbol{\omega} &= \dot{\varphi}_1 \mathbf{e}_1^1 + \dot{\psi}_1 \mathbf{n}_1, \\ \boldsymbol{\omega}^2 &= \dot{\varphi}_1^2 + \dot{\psi}_1^2 = \dot{\varphi}_1^2 \frac{1 - S^2 c^2(1 + S^2 s^2)}{(1 - S^2 c^2)^2}. \end{aligned} \right\} \tag{13.29}$$

With these expressions and with  $\mathbf{v}_A = \dot{z}_1 \mathbf{n}_1$  (13.27) yields

$$\mathbf{u} = \ell \frac{c(C^2 - S^2 s^2)}{1 - S^2 c^2(1 + S^2 s^2)} (-s \mathbf{e}_2^1 + c \mathbf{e}_3^1). \tag{13.30}$$

This expression and the expressions for  $\boldsymbol{\omega}$  and for  $z_1$  are substituted into (13.26). The coordinates of  $\boldsymbol{\omega}$  in the bases  $\mathbf{e}^1$  and  $\mathbf{n}$  are known from (13.16) and (13.13), respectively. The coordinates of  $\mathbf{e}_2^1$  and of  $\mathbf{e}_3^1$  in  $\mathbf{n}$  are calculated from (13.3) and (13.5). Substitution of all these expressions results in the desired parameter equations for the axodes:

Fixed axode in basis $\mathbf{e}_{1,2,3}^1$ :	moving axode in basis $\mathbf{n}_{1,2,3}$ :
$\ell \begin{bmatrix} \lambda \\ \frac{-cs(C^2 - S^2 s^2)}{1 - S^2 c^2(1 + S^2 s^2)} + \lambda \frac{CS c^2}{1 - S^2 c^2} \\ \frac{c^2(C^2 - S^2 s^2)}{1 - S^2 c^2(1 + S^2 s^2)} + \lambda \frac{CS cs}{1 - S^2 c^2} \end{bmatrix},$	$\ell \begin{bmatrix} \frac{-s + \lambda CS c}{1 - S^2 c^2} \\ \frac{-1}{\sqrt{1 - S^2 c^2}} \left[ \frac{Cc(C^2 - S^2 s^2)}{1 - S^2 c^2(1 + S^2 s^2)} + \lambda S s \right] \\ \frac{1}{\sqrt{1 - S^2 c^2}} \left[ \frac{S cs(C^2 - S^2 s^2)}{1 - S^2 c^2(1 + S^2 s^2)} - \lambda C \right] \end{bmatrix}.$
	(13.31)

In Fig. 13.5 the axodes for the parameter value  $\alpha = 60^\circ$  are shown (the fixed axode dark, the white moving axode in a single position). Each axode is represented by a net of lines  $\lambda = \text{const}$  ( $-2 \leq \lambda \leq 2$ ) and  $\varphi_1 = \text{const}$ . The moving axode is raccording around the fixed axode twice per revolution of shaft 1. For showing the moving axode in a single position  $\varphi_1 = \phi$  together with the fixed axode the coordinates in the column matrix on the right-hand side of (13.31) are transformed into basis  $\mathbf{e}^1$ . The transformation matrix for this purpose is composed of the three columns shown in (13.3) with  $\varphi_1 = \phi$ . To the resulting coordinates the coordinates of the vector  $\mathbf{r}_{AM}(\phi) = z_1(\phi) \mathbf{n}_1(\phi)$  are added (see (13.26)). The raccording motion is made visible by showing the moving axode in a sequence of pictures over the full range of values  $0 \leq \phi \leq 2\pi$ .

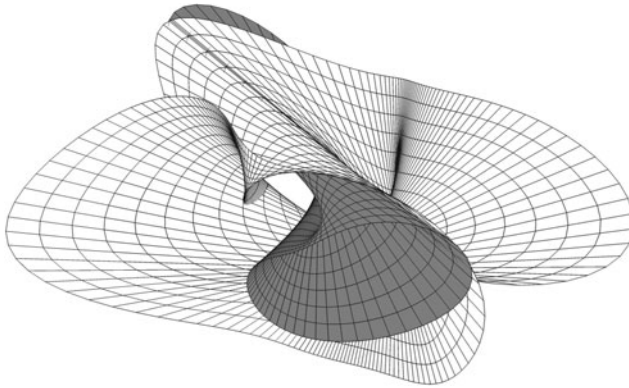


Fig. 13.5 Raccording axodes of the central ring for  $\alpha = 60^\circ$  (fixed axode dark)

### 13.3 Series-Connected Hooke's Joints

Equation (13.7) has shown that the output angular velocity of Hooke's joint is oscillating if the input angular velocity is constant. For this reason the single Hooke's joint has a limited range of engineering applications. The present section is devoted to the following problem. A chain of shafts  $1, \dots, n$  is interconnected by Hooke's joints  $1, \dots, n - 1$ . The shafts labeled 1 and  $n$  are referred to as input shaft and as output shaft, respectively. The entire system between these two shafts represents a single joint. To be formulated are necessary and sufficient conditions guaranteeing the angular velocity ratio  $\dot{\varphi}_n / \dot{\varphi}_1 \equiv 1$ .

First, the case  $n = 3$  is investigated, i.e., the case of Hooke's joints 1 and 2 coupling shafts 1, 2 and 3. The parameter  $\alpha$  of Fig. 13.1 associated with Hooke's joint 1 is now called  $\alpha_1$ . The parameter  $\alpha_2$  associated with Hooke's joint 2 is the constant angle between shafts 2 and 3. Until further below it is assumed that shafts 1, 2 and 3 are coplanar. Since they are coplanar, only two configurations are possible in which shafts 1 and 3 intersect at an angle which is either  $\alpha_1 + \alpha_2$  or  $\alpha_1 - \alpha_2$ . The cross of each of the two Hooke's joints is rotating relative to shaft 2 about an axis which is perpendicular to shaft 2. Let  $\beta_2$  be the constant angle between these two perpendiculars. It is a third parameter in addition to  $\alpha_1$  and  $\alpha_2$ . The sign of  $\beta_2$  is specified by the definition that  $\varphi_2 - \beta_2$  is the input angle of the second Hooke's joint. Applying (13.4) to both joints results in the relationships

$$\tan \varphi_2 \tan \varphi_1 = -\cos \alpha_1, \quad \tan \varphi_3 \tan(\varphi_2 - \beta_2) = -\cos \alpha_2. \quad (13.32)$$

In what follows, only the special cases  $\beta_2 = 0$  and  $\beta_2 = \pi/2$  are considered. With the identity  $\tan \psi = -\cot(\psi - \pi/2)$  the second Eq.(13.32) is given the form

$$\left. \begin{aligned} \beta_2 = 0 : \quad & \cot(\varphi_3 - \frac{\pi}{2}) \tan \varphi_2 = \cos \alpha_2 , \\ \beta_2 = \frac{\pi}{2} : \quad & \tan \varphi_3 \cot \varphi_2 = \cos \alpha_2 . \end{aligned} \right\} \quad (13.33)$$

Combination with the first Eq.(13.32) eliminates  $\varphi_2$ . The result is the desired input-output relationship

$$\left. \begin{aligned} \beta_2 = 0 : \quad & \tan(\varphi_3 - \frac{\pi}{2}) \tan \varphi_1 = -\cos \alpha_1 / \cos \alpha_2 , \\ \beta_2 = \frac{\pi}{2} : \quad & \tan \varphi_3 \tan \varphi_1 = -\cos \alpha_1 \cos \alpha_2 . \end{aligned} \right\} \quad (13.34)$$

This is written in the form

$$\tan(\varphi_3 - \gamma_3) \tan \varphi_1 = -a_3 , \quad a_3 = \begin{cases} \cos \alpha_1 / \cos \alpha_2 & (\beta_2 = 0) \\ \cos \alpha_1 \cos \alpha_2 & (\beta_2 = \frac{\pi}{2}) \end{cases} \quad (13.35)$$

with either  $\gamma_3 = \pi/2$  or  $\gamma_3 = 0$ .

The generalization to chains with  $n - 1$  Hooke’s joints coupling shafts  $1, \dots, n$  is straight-forward. Again, the shafts are assumed to be coplanar. With each new shaft  $i$  a new shaft parameter  $\beta_{i-1}$  (either  $\beta_{i-1} = 0$  or  $\beta_{i-1} = \pi/2$ ) and a new joint parameter  $\alpha_{i-1}$  are introduced and with them a new equation of the general form (13.33) with indices  $i$  and  $i - 1$  instead of 3 and 2. The angle  $\varphi_{i-1}$  is eliminated by combining this equation with the previous equation of the general form (13.35). The final result for the input-output relationship for a chain of  $n - 1$  Hooke’s joints coupling shafts  $1, \dots, n$  has the form

$$\tan(\varphi_n - \gamma_n) \tan \varphi_1 = -a_n \quad (13.36)$$

with constants  $\gamma_n$  and  $a_n$ . The latter is

$$a_n = \cos \alpha_1 \prod_{i=2}^{n-1} (\cos \alpha_i)^{\nu_i} , \quad \nu_i = \begin{cases} +1 & (\beta_i = \frac{\pi}{2}) \\ -1 & (\beta_i = 0) \end{cases} \quad (n \geq 3) . \quad (13.37)$$

Differentiation with respect to time yields the angular velocity ratio (compare the transition from (13.4) to (13.7))

$$\frac{\dot{\varphi}_n}{\dot{\varphi}_1} = \frac{a_n}{1 - (1 - a_n^2) \cos^2 \varphi_1} . \quad (13.38)$$

The desired angular velocity ratio  $\dot{\varphi}_n/\dot{\varphi}_1 \equiv 1$  is achieved with  $a_n = 1$ . This is a condition on the joint parameters  $\alpha_1, \dots, \alpha_{n-1}$  and on the shaft parameters  $\beta_2, \dots, \beta_{n-1}$ .

**Example  $n = 3$ :** Equation (13.35) shows that  $a_3 = 1$  requires  $\beta_2 = 0$  and, in addition,  $\cos \alpha_1 / \cos \alpha_2 = 1$ , i.e.,  $|\alpha_1| = |\alpha_2|$ . This result was to be expected. In [Figs. 13.6a](#) and [b](#) the two possible arrangements with coplanar shafts 1, 2 and 3 are shown.



**Fig. 13.6** The two possible couplings of coplanar shafts 1, 2, 3 by two Hooke's joints resulting in  $\dot{\varphi}_3 \equiv \dot{\varphi}_1$

At this point the condition of coplanarity of the three shafts is abandoned. Obviously, the property  $\dot{\varphi}_3 \equiv \dot{\varphi}_1$  is preserved if the planar system (for example, the one in Fig. 13.6a) is subjected to the following three-step operation:  
 Step 1: In an arbitrary position shaft 2 is cut thus splitting the entire system into a left part 1 and a right part 2  
 Step 2: Part 2 including joint 2 and the bearing of shaft 3 is rotated as one single rigid body about the axis of shaft 2 through an arbitrary angle  $\psi$   
 Step 3: In the new position  $\psi$  the two parts of shaft 2 are rigidly joined together.

In the special case  $\psi = \pi$ , the new position is the position shown in Fig. 13.6b. If  $\psi \neq \pi$ , the axes of shafts 1 and 3 are skew in the new position.

**Example  $n = 4$ :** Equation (13.37) shows that the condition  $a_4 = 1$  is satisfied in each of the following three cases.

Case a:  $(\beta_2, \beta_3) = (\frac{\pi}{2}, 0)$  and  $\cos \alpha_1 \cos \alpha_2 = \cos \alpha_3$

Case b:  $(\beta_2, \beta_3) = (0, 0)$  and  $\cos \alpha_2 \cos \alpha_3 = \cos \alpha_1$

Case c:  $(\beta_2, \beta_3) = (0, \frac{\pi}{2})$  and  $\cos \alpha_3 \cos \alpha_1 = \cos \alpha_2$ .

In Fig. 13.7 case (c) is illustrated by a system of coplanar axes with  $\alpha_3 = \alpha_1 = 20^\circ$  and  $\cos \alpha_2 = \cos^2 20^\circ$  ( $\alpha_2 \approx 28^\circ$ ). This example shows that geometrical symmetry of the coupling of shafts 1 and 4 is not a necessary condition for the identity of input and output angular velocity.

**Example  $n = 5$ :** The condition  $a_5 = 1$  is satisfied by altogether seven different combinations  $(\beta_2, \beta_3, \beta_4)$  and by associated conditions on  $\alpha_1, \dots, \alpha_4$ . The details are left to the reader. See also Duditza [4, 7]. In Fig. 13.8 a simple example with five coplanar axes is shown. It is the combination of two systems of the type shown in Fig. 13.6b. The parameters are  $\beta_2 = \beta_3 = \beta_4 = 0$  and  $\alpha_1 = \alpha_2 = \alpha_3 = \alpha_4 = \alpha$ . Shafts 1, 3 and 5 have identical angular velocities  $\dot{\varphi}_5 \equiv \dot{\varphi}_3 \equiv \dot{\varphi}_1$ .

In every system with coplanar axes  $i = 1, \dots, n$  the property  $\dot{\varphi}_n \equiv \dot{\varphi}_1$  is preserved if the three-step operation explained for the case  $n = 3$  is applied analogously, i.e., by cutting an arbitrary intermediate shaft  $j = 2, \dots, n - 1$  and by a rigid-body rotation of the part located beyond the cut shaft. This operation may even be performed repeatedly with different intermediate shafts.

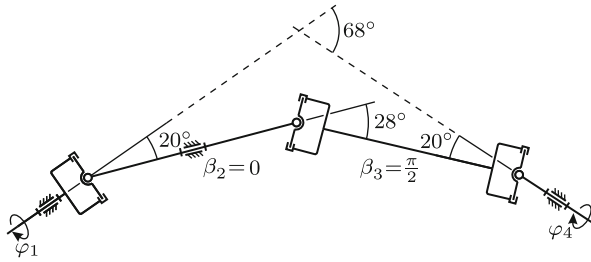


**Fig. 13.7** Unsymmetrical coupling of coplanar shafts 1, 2, 3, 4 by three Hooke's joints resulting in  $\dot{\varphi}_4 \equiv \dot{\varphi}_1$

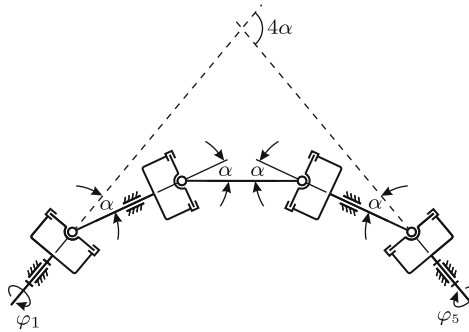


**Fig. 13.8** Coupling of coplanar shafts 1, 2, 3, 4, 5 by four Hooke's joints resulting in  $\dot{\varphi}_5 \equiv \dot{\varphi}_3 \equiv \dot{\varphi}_1$

### 13.4 Homokinetic Shaft Couplings

By definition, the coupling of two shafts is homokinetic if it satisfies the conditions

(A) the axes of the shafts are free to change their relative position and direction during operation

(B) the angular velocities are identical in *every* relative position and direction held fixed.

The homokinetic coupling is the mechanism required for positioning and directing the axis of shaft 2 relative to shaft 1. If both location and direction of this axis are variable, the mechanism must have the degree of freedom  $F = 5$  (three coordinates of a single point plus two direction cosines). Couplings of simpler nature, namely, with degree of freedom  $F = 2$ , are required for shafts the axes of which are permanently intersecting at a fixed point. In engineering these simpler solutions are fully sufficient. Such coupling cannot be a serial chain because it would have to be a chain of two intersecting revolute joints. However, this is Hooke's joint which is known to violate condition (B). This means that homokinetic couplings must be closed kinematic chains.

### 13.4.1 Couplings With a Spherical Joint

Permanent intersection of the axes of shafts 1 and 2 is most easily achieved by means of a spherical joint. According to Grübler's Eq.(4.4) a simple closed chain with a spherical joint must have five additional joint variables in order to have the degree of freedom  $F = 2$ . Let  $\Sigma$  be the plane which is (i) bisecting the angle between the two shafts and (ii) normal to the plane spanned by the shafts. Conditions (A) and (B) are both satisfied if in every relative position of the shafts the closed chain is both structurally and dimensionally symmetric with respect to  $\Sigma$ . If only revolute joints R, prismatic joints P and combinations of these two (cylindrical joints C, spherical joints S and planar joints E) are used, altogether eight five-variable chains can be formed which are structurally symmetric with respect to a central joint. These are the chains **R**RRRR, R**R**PRR, PRR**R**P, R**P**RPR, **R**SR, **P**SP, **C**RC and **R**ER. The central joint is indicated by a boldface letter. If the central joint is a revolute R, its axis must lie in  $\Sigma$ . If it is a prismatic joint P, it must be perpendicular to  $\Sigma$ . If it is a planar joint E, the plane E must be normal to  $\Sigma$ . Every one of the eight mechanisms has been used in patented shaft couplings. Detailed documentations see in Kutzbach [10, 11], Duditzka [5] and Seherr-Thoss/Schmelz/Aucktor [17]. In most engineering realizations adjacent joint axes are either parallel or at right angles. This is not a necessary condition. The only necessary condition, in addition to symmetry, is that the shafts must have the freedom to rotate full cycle.

A homokinetic coupling based on the chain **R**SR was shown in Fig. 4.11. A coupling based on the chain **C**RC is shown schematically in Fig. 13.9a. It was known to Koenigs [9] already. The patented engineering realization is known as Hebson coupling. A single chain **C**RC suffices. The second chain **C**RC is added in order to diminish dynamical unbalance (total balance is achieved when shafts 1 and 2 are collinear). In a Hebson coupling a larger number of chains is evenly distributed around the cylinders. The joints R in these chains may be replaced by spherical joints since the additional degrees of freedom thus introduced are passive. With this coupling inclination angles up to  $90^\circ$  are possible.

The so-called Tracta coupling shown schematically in Fig. 13.9b is based on the chain **R**ER. The chain is encapsulated in two concentric spherical shells which together represent the spherical joint connecting shafts 1 and 2. The axes of both revolute R are in the plane E. Each revolute axis intersects one shaft axis orthogonally. Rotations in these revolute keep plane E normal to plane  $\Sigma$  independent of the angular position  $\varphi$  of the shafts. In the figure plane E is shown in the positions  $\varphi = 0, \pi$  and  $\varphi = \pm\pi/2$ . The Tracta coupling is widely used in the automotive field because of the following properties: Inclination angles up to  $50^\circ$ ; compact form; simple assembly; no loss of lubrication; large wear-resistant contact surfaces.

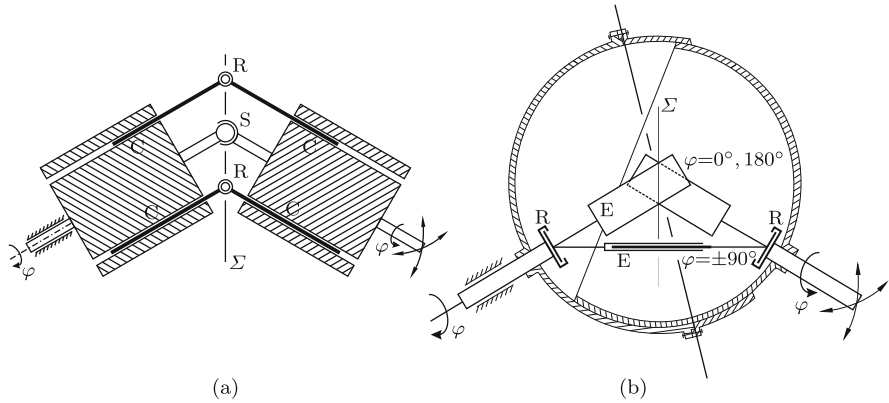


**Fig. 13.9** Hebson coupling (a) and Tracta coupling (b)

In the homokinetic coupling shown in Fig. 13.10 two involutes on either side of plane  $\Sigma$  constitute the central cross of a Hooke's joint each connecting one shaft to the intermediate body 3. For this reason the coupling is referred to as bicardanic coupling. Body 3 is a cylinder with the axis  $0_1-0_2$  inside of which centrally placed rings 4 provide a planar joint in plane  $\Sigma$  for the smaller circular disc 5. Normal to this disc another hollow cylinder 6 is rigidly connected. This cylinder is guide for two spherical bodies fixed at the ends of shafts 1 and 2 at equal distances from  $0_1$  and from  $0_2$ , respectively. The entire mechanism connecting shafts 1 and 2 is homokinetic. The point of intersection of the shafts is not fixed on the shafts, but constrained to lie in  $\Sigma$ . This type of coupling finds applications in low-speed vehicles such as agricultural machines. For high-speed vehicles it is not suitable because the nonuniform motion of the coupling mechanism is a source of vibrations.

Duditza [4, 5] and Kutzbach [10] describe various other forms of bicardanic homokinetic couplings.

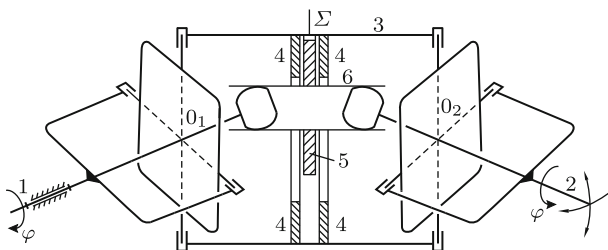


**Fig. 13.10** Bicardanic homokinetic coupling

### 13.4.2 Couplings With Three Parallel Serial Chains

In the shaft couplings described in the previous section permanent symmetry of a five-d.o.f. chain with respect to plane  $\Sigma$  is achieved by a central spherical joint  $S$  closing the chain. The same constraints that are exerted by the spherical joint  $S$  can be exerted by placing two additional five-d.o.f. chains parallel to the first one. For reasons of dynamic balancing and of simplicity of design three identical chains are placed at intervals of  $120^\circ$ . The so-called Clemens coupling shown schematically in Fig. 13.11 is derived from Fig. 4.11. The serial chain  $R_1S_2R_2$  of this coupling is placed three times in parallel. On each shaft the three revolute axes fixed on the shaft are placed  $120^\circ$  apart. The three spherical joints are permanently in the bisecting plane  $\Sigma$ .

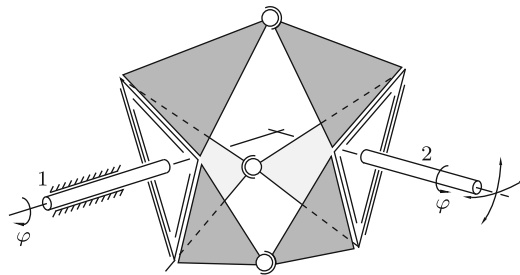


Fig. 13.11 Clemens coupling with three identical parallel chains RSR

The shafts 1 and 2 in Fig. 13.12 are connected to the sides of the rigid isosceles triangle  $(0_1, C, 0_2)$  of base length  $2\ell$  and apex angle  $2\beta$  by two pairs of revolutes  $R_1, R_2$  and  $R_3, R_4$ . At  $0_1$  the axis of  $R_1$  intersects both shaft 1 and  $R_2$  orthogonally, and at  $0_2$  the axis of  $R_4$  intersects both shaft 2 and  $R_3$  orthogonally. In the figure the symmetrical position is shown in which the shafts intersect in the bisecting plane  $\Sigma$  normal to  $\overline{0_1 0_2}$  and passing through  $C$ . When the shafts are held fixed in this position, rotation of the triangle about the line  $\overline{0_1 0_2}$  causes both shafts to rotate through identical angles  $\varphi$ . The chain  $R_1R_2R_3R_4$  is one out of three identical chains sharing the line  $\overline{0_1 0_2}$  and the plane  $\Sigma$ . The entire shaft coupling thus described is known as Unitru coupling. It is homokinetic because it allows changing the direction of shaft 2 while maintaining symmetry with respect to  $\Sigma$ .

In what follows, it is shown under which condition on the design parameter  $\beta$ , for a given inclination angle  $\alpha$  of the shafts, the triangle and the shafts are free to rotate full cycle. Definition: The angle of rotation  $\varphi$  of the shafts and the angle of rotation  $\psi$  of the triangle are zero when the shafts as well as the triangle are in the plane of the drawing (the frame-fixed  $x, y$ -plane). In this position the revolutes  $R_1$  and  $R_4$  are parallel to the  $z$ -axis. The point  $P$  on the axis of  $R_4$  at the distance  $\ell$  from  $0_2$  is an auxiliary point. With

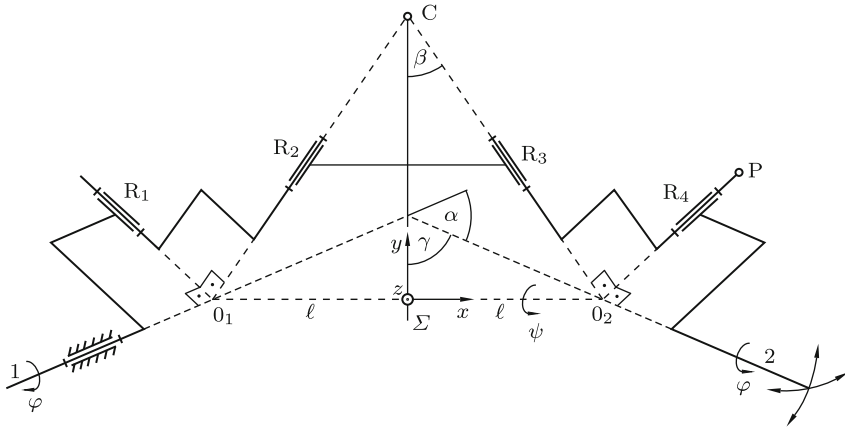


Fig. 13.12 Single serial chain of a Unitru coupling

the altitude  $l \cot \beta$  of the triangle the  $x, y, z$ -coordinates of C and P are

$$\left. \begin{aligned} C(\psi, \beta) : & \quad \ell[0 \qquad \qquad \qquad \cos \psi \cot \beta \quad \sin \psi \cot \beta], \\ P(\varphi, \gamma) : & \quad \ell[1 - \sin \varphi \cos \gamma \quad -\sin \varphi \sin \gamma \quad \cos \varphi]. \end{aligned} \right\} \quad (13.39)$$

The distance between C and P is  $\ell\sqrt{2 + \cot^2 \beta}$  independent of  $\psi$  and  $\varphi$ . This condition yields the equation

$$\cos \psi \sin \varphi \sin \gamma - \sin \psi \cos \varphi = \tan \beta \sin \varphi \cos \gamma. \quad (13.40)$$

It has the form  $A \cos \psi + B \sin \psi = R$ . The triangle can rotate full cycle if  $A^2 + B^2 - R^2 \geq 0$  for  $0 \leq \varphi \leq 2\pi$ . This is the condition

$$1 - \frac{\cos^2 \gamma}{\cos^2 \beta} \sin^2 \varphi \geq 0. \quad (13.41)$$

This requires  $\cos \beta \geq \cos \gamma$  or  $\beta \leq \gamma \leq \pi/2$ . The inclination angle between the two shafts is  $\alpha = \pi - 2\gamma$ . Thus, the condition is  $2\beta \leq \pi - \alpha$ . With  $2\beta = 90^\circ$  inclination angles  $\alpha$  up to  $90^\circ$  are possible.

### 13.4.3 Ball-in-Track Joints

The symmetrical five-d.o.f. chains essential for all previously described shaft couplings have the disadvantage of being structurally complex. Much simpler realizations are shown in Figs. 13.13a and b. The shafts in Fig. 13.13a are connected by a spherical joint. The shafts as well as the symmetrical curves

of arbitrary shape drawn in thick lines are in the plane of the drawing. Imagine these curves to be rigid and rigidly attached to the shafts. Due to the symmetry the point of contact is in the bisecting plane  $\Sigma$ . Both symmetry with respect to and contact in the bisecting plane are maintained when the inclination angle  $\alpha$  between the shafts is changed and also, when both shafts are rotated through arbitrary identical angles into positions in which the two curves are no longer coplanar. The sliding point contact of two curves constitutes a five-d.o.f. joint. The symmetrical closed chain formed by this joint in parallel to the spherical joint represents a homokinetic coupling of shafts 1 and 2. However, since point contact is transmitting force from one shaft to the other in only one sense of direction of rotation, a second pair of rigid curves for the opposite sense of direction is necessary. This is the pair drawn in dashed lines in the same plane. Repeating the arguments at the beginning of the previous section the shaft coupling continues to be homokinetic if the central spherical joint is replaced by two additional sets of curves in planes placed at intervals of  $120^\circ$ . Engineering realizations see in Kutzbach [10]. The contacting curves are edges of bodies.

Single-point contact of curves is unsatisfactory. A much better design is the so-called ball-in-track joint shown in Fig. 13.13b. The role of the contact point is played by the center C of a spherical ball of arbitrary diameter. Motion of C relative to the shafts along prescribed symmetric curves is realized by appropriately curved shallow grooves referred to as tracks in which the ball is constrained to move. Each track is rigidly attached to one of the shafts. The element composed of a ball enclosed between two crossing tracks is called ball-in-track joint. It is a five-d.o.f. joint. Homokinetic shaft couplings with ball-in-track joints have many advantages such as small size, small dynamic unbalance and distribution of contact forces among a large number of balls. However, there are disadvantages, too. Problems arise from the fact that the motion of balls in crossing tracks is not rolling, but sliding and boring with the possibility of jamming due to friction. This aspect of kinematics see in Phillips/Winter [14].

The so-called Devos coupling shown schematically in Fig. 13.14 has two balls-in-tracks in parallel to a spherical joint S. The tracks are symmetrically located cylinders. In order to keep the centers of the balls in the bisecting plane  $\Sigma$  the balls are also constrained to move along the cylindrical pin 3 which is rigidly attached to the sphere of the joint S. This implies that the sphere of the joint S cannot be rigidly connected to any of the two shafts. Details of design not shown in the figure allow the shaft coupling to be assembled under prestress in such a way that its elements are firmly held together.

Figure 13.15 shows the essential elements of a shaft coupling without central spherical joint and with balls in torus-shaped tracks in the particular position when the circular lines of contact between ball and both tori (indi-

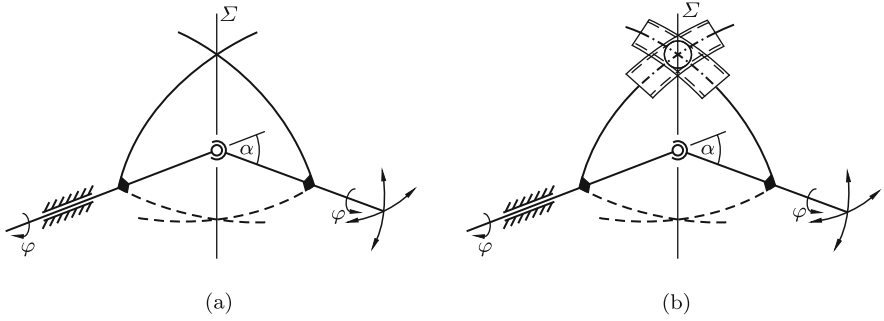


**Fig. 13.13** Homokinetic coupling with contacting symmetrical curves (a) and with a ball-in-track joint (b)

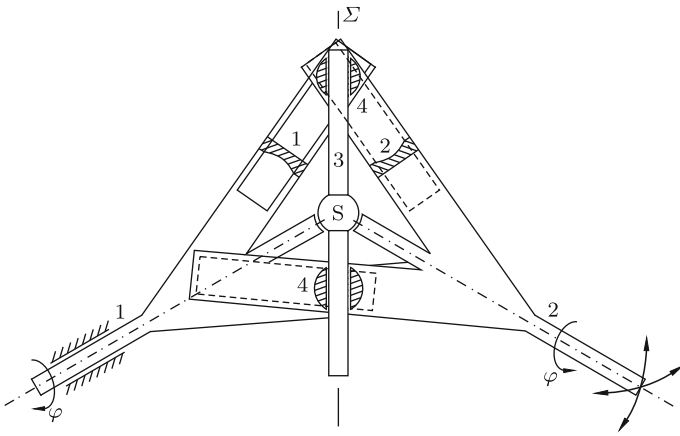


**Fig. 13.14** Devos coupling with balls in cylindrical tracks

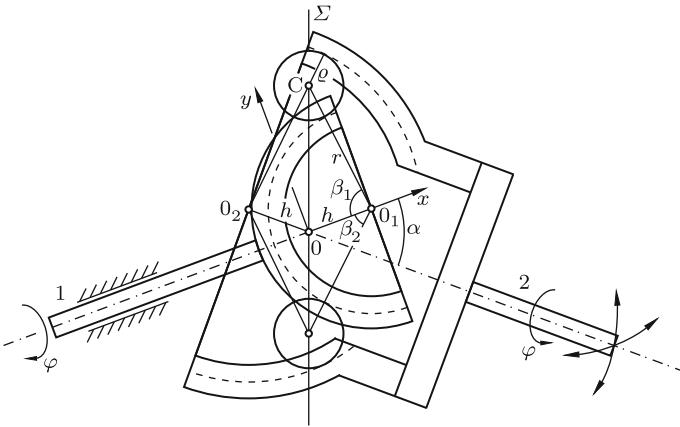


**Fig. 13.15** Homokinetic shaft coupling with balls in torus-shaped tracks

cated by the dashed circles) are in the plane of the drawing<sup>4</sup>. Let this be the position  $\varphi = 0$  of the shafts. The radii  $r_1$  and  $r_2$  of these circles satisfy the condition  $r_2 - r_1 = 2\rho$  where  $\rho$  is the radius of the balls. This has the effect that the trajectory of the center  $C$  of the ball relative to shaft 1 is the circle of radius  $r = r_1 + \rho$  about  $O_1$  and that the trajectory of  $C$  relative to shaft 2 is the circle of the same radius  $r$  about  $O_2$ . In the position  $\varphi = 0$  these circles are symmetric with respect to and intersecting in the bisecting plane  $\Sigma$ . The pair of balls shown in the figure is one out of three or more pairs moving in tracks which are placed at equal angular intervals. After what has been said in the context of Figs. 13.13a,b the symmetry properties prove that the shaft coupling is homokinetic. Not only in the position  $\varphi = 0$ , but in arbitrary positions  $\varphi \neq 0$  point  $C$  is in the plane  $\Sigma$  at equal distances  $r$  from  $O_1$  and from  $O_2$ . Hence the trajectory of  $C$  relative to the frame is a circle in  $\Sigma$  with the center at the midpoint between  $O_1$  and  $O_2$ . The radius of this circle depends on  $\alpha$ .

The position of  $C$  in the tracks is described by the angle  $\beta = \sphericalangle(0O_1C)$ . It is a function  $\varphi$ . The extremal values  $\beta_1$  and  $\beta_2$  are obtained from the condition that the  $x, y$ -coordinates of  $C$  satisfy the equation  $x = y \tan \alpha/2$ . This is the set of equations

$$h - r \cos \beta_{1,2} = \pm r \sin \beta_{1,2} \tan \frac{\alpha}{2}. \tag{13.42}$$

Solving for  $\sin \beta_{1,2}$  results in the formulas

$$\sin \beta_{1,2} = \frac{(h/r) \tan \alpha/2 \pm \sqrt{1 + \tan^2 \alpha/2 - (h/r)^2}}{1 + \tan^2 \alpha/2}. \tag{13.43}$$

An animation of the motion is on display in *Wikipedia Homokinetisches Gelenk*.

### 13.4.4 Tripod Joint

The tripod joint shown in Fig. 13.16 is another ball-in-track coupling. Its kinematics was investigated by Roethlisberger/Aldrich [16], Duditzka [5], Duditzka/Diaconescu [6], Durum [8], Orain [12, 13] and Akbil/Lee [1, 2]. In what follows, an elementary analysis is presented. Imagine that in the fixed cartesian  $x_1, y_1, z_1$ -system of Fig. 13.17 the shaft labeled 1 is rotating about the  $z_1$ -axis. The rotation angle is  $\varphi$ . A point  $Q$  fixed on the shaft at radius  $a$  is moving on a circle. In the position  $\varphi$  of the shaft  $Q$  has the coordinates  $x_1(\varphi) = a \cos \varphi$ ,  $y_1(\varphi) = a \sin \varphi$ . The circle and this point  $Q(\varphi)$  are

<sup>4</sup> The dimensions chosen in the figure are unrealistic because they allow only small variations of the angle  $\alpha$

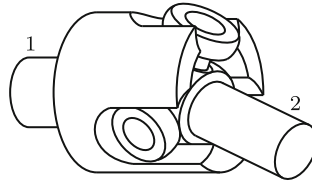


**Fig. 13.16** Tripod joint. Balls sliding on the rays of the star-shaped tripod 2 are guided in tracks fixed on shaft 1

projected parallel to the  $z_1$ -axis onto the  $x, y$ -plane of another fixed  $x, y, z$ -system which is inclined against the  $x_1, y_1, z_1$ -system by an angle  $\alpha$  about the  $x_1$ -axis. The projection of the circle is the ellipse with semi-axes  $a$  and  $b = a / \cos \alpha$ . Point  $Q(\varphi)$  is projected into the point  $P(\varphi)$  with coordinates

$$x(\varphi) = a \cos \varphi, \quad y(\varphi) = b \sin \varphi. \tag{13.44}$$

Let, in the same  $x, y$ -plane,  $x_0(\varphi)$  and  $y_0(\varphi)$  be the coordinates of another point  $P_0(\varphi)$ , i.e., of another curve. To be determined are all curves  $P_0(\varphi)$  having the property that the angle between the line  $\overline{P_0(\varphi)P(\varphi)}$  and the  $x$ -axis is identical with  $\varphi$ . This is the condition

$$\frac{b \sin \varphi - y_0(\varphi)}{a \cos \varphi - x_0(\varphi)} \equiv \tan \varphi. \tag{13.45}$$

The ansatz

$$x_0(\varphi) = \xi(\varphi) \cos \varphi, \quad y_0(\varphi) = \eta(\varphi) \sin \varphi \tag{13.46}$$

results in the condition

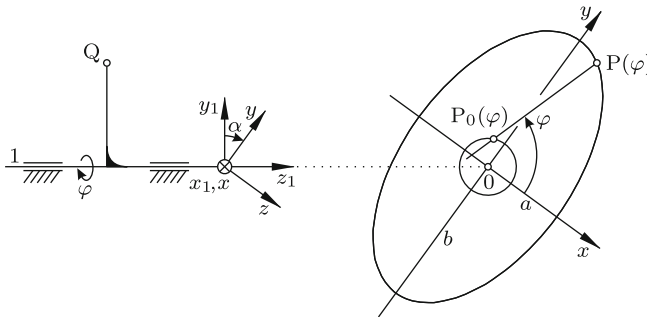


**Fig. 13.17** Point  $Q$  fixed at radius  $a$  on the rotating shaft 1 (rotation angle  $\varphi$ ) is projected parallel to the  $z_1$ -axis into the point  $P(\varphi)$  in the fixed  $x, y$ -plane. Another point  $P_0(\varphi)$  in the  $x, y$ -plane

$$\eta(\varphi) - \xi(\varphi) \equiv b - a. \tag{13.47}$$

This condition is satisfied by infinitely many functions, for example, by the family of functions  $\xi(\varphi) = -r(\cos^2 \varphi + c_1)$ ,  $\eta(\varphi) = r(\sin^2 \varphi + c_2)$  with constants  $r, c_1, c_2$  satisfying the constraint equation  $r(1 + c_1 + c_2) = b - a$ . In the special case  $c_1 = c_2 = -3/4$ ,  $r = -2(b - a)$ , Eqs.(13.46) are

$$\left. \begin{aligned} x_0(\varphi) &= \varrho \cos 3\varphi, & y_0(\varphi) &= \varrho \sin 3\varphi, \\ \varrho &= -\frac{r}{4} = \frac{b - a}{2} = a \frac{1 - \cos \alpha}{2 \cos \alpha}. \end{aligned} \right\} \tag{13.48}$$

When shaft 1 is rotating with angular velocity  $\dot{\varphi}$ ,  $P_0(\varphi)$  is moving with angular velocity  $3\dot{\varphi}$  on the circle with radius  $\varrho$  about 0, and the line  $P_0(\varphi)P(\varphi)$  is rotating with angular velocity  $\dot{\varphi}$ . Examples:  $\varrho \approx 0.08a$  for  $\alpha = 30^\circ$ ,  $\varrho \approx 0.21a$  for  $\alpha = 45^\circ$ ,  $\varrho = 0.5a$  for  $\alpha = 60^\circ$ . The Taylor formula is  $\varrho/a \approx \alpha^2/4$ .

Imagine that on the circle of radius  $a$  fixed on shaft 1 not a single point  $Q$ , but three points  $Q_1, Q_2, Q_3$  are marked  $120^\circ$  apart. The projections of these points are three points  $P_i(\varphi)$  ( $i = 1, 2, 3$ ) on the ellipse. For each one of these points (13.48) yields the same point  $P_0(\varphi)$  since  $3 \cdot 120^\circ = 2\pi$ . From this it follows that the rays  $\overline{P_0(\varphi)P_i(\varphi)}$  ( $i = 1, 2, 3$ ) emanating from  $P_0(\varphi)$  form a rigid  $120^\circ$ -star with the center at  $P_0$ . This star is rotating with angular velocity  $\dot{\varphi}$  while its center  $\overline{P_0}$  is moving on the circle of radius  $\varrho$  with angular velocity  $3\dot{\varphi}$ . The lines  $\overline{Q_i(\varphi)P_i(\varphi)}$  ( $i = 1, 2, 3$ ) are parallel to the axis of shaft 1 and fixed on shaft 1. In the tripod joint shown in Fig. 13.16 the star, the three lines  $\overline{Q_i(\varphi)P_i(\varphi)}$  ( $i = 1, 2, 3$ ) and the permanent intersection of each ray with the associated line at  $P_i$  are materially realized. Each ray is guide for a ball which is free to move along the ray. The associated line fixed on shaft 1 is the axis of a cylinder in which the ball is also free to move. Orthogonal to the star and through its center  $P_0$  a shaft 2 is rigidly attached to the star. The star and this shaft together constitute the tripod giving the joint its name. The tripod has the same angular velocity  $\dot{\varphi}$  shaft 1 has independent of the direction of shaft 2 relative to shaft 1. It has the additional degree of freedom of translation along the axis of shaft 1. In spite of these properties the tripod joint is not homokinetic because shaft 2 cannot be held fixed due to its motion on a cylinder of radius  $\varrho$ . By means of an Oldham coupling the motion of shaft 2 can be transmitted to a shaft 3 the axis of which is the  $z$ -axis. This combination tripod joint – Oldham coupling is a homokinetic coupling of shafts 1 and 3.

If a point fixed on shaft 2 at a distance  $\ell \gg a$  from  $P_0$  is coupled to the  $z$ -axis by a spherical joint  $S$ , the kinematics of the tripod is slightly changed. An analysis made by Duditza and Diaconescu [5, 6] leads to the following first-order approximation. Three times per revolution of shaft 1 the axis of shaft 2 is moving on a circular cone with the apex at  $S$  and with the semi-

vertex angle  $\varrho/\ell \ll 1$ , and the angular velocity of the tripod about shaft 2 is approximately  $\dot{\varphi}(1 - A \cos 3\varphi)$  with  $A = \frac{3}{2}(a/\ell) \tan \alpha \tan^2 \alpha/2 \ll 1$ .

## References

1. Akbil E, Lee T W (1983) Kinematic structure and functional analysis of shaft couplings involving poded joints. *J. Mechanisms, Transm., Automation in Design* 105:672–681
2. Akbil E, Lee T W (1984) On the motion characteristics of tripode joints. Part 1: General case. Part 2: Applications. *J. Mechanisms, Transm., Automation in Design*, 106:228–234 and 235–245
3. Balken J (1981) Systematische Entwicklung von Gleichlaufgelenken. Diss. TU München
4. Duditz F (1973) Kardangelenkgetriebe und ihre Anwendungen. VDI-Verl., Düsseldorf
5. Duditz F (1974) Cuplaje mobile homocinetice. Tehnica, Bucarest
6. Duditz F, Diaconescu D (1975) Zur Kinematik und Dynamik von Tripode-Gelenkgetrieben. *Konstruktion* 27:335–341
7. Duditz F, Diaconescu D, Böhm C, Saulescu R (2003) Transmisii cardanice. Editura Transilvania Expres 2003
8. Durum M M (1975) Kinematic properties of tripode joints. *J. Eng. Ind.* 97B:708–713
9. Koenigs G (1897) Leçons de cinématique. Avec des notes par G. Darboux, E. et F. Cosserat. Hermann, Paris
10. Kutzbach K (1937) Quer- und winkelbewegliche Wellenkupplungen. *Kraftfahrtechnische Forschungsarbeiten* 6:1–25
11. Kutzbach K (1937) Quer- und winkelbewegliche Gleichganggelenke für Wellenleitungen. *VDI-Zeitschr.* 81:889–892
12. Orain M (1976) Contribution à l'étude des joints de transmission tripodes. Diss. Univ. Pierre et Marie Curie, Paris
13. Orain M (1977) Allgemeine Theorie und experimentelle Forschung der Gleichlaufgelenke. Glaenzer Spicer, Poissy, France
14. Phillips J R, Winter H (1968) Über die Frage des Gleitens in Kugel-Gleichganggelenken. *VDI Z.* 110:228–233
15. Poncelét J V (1836) Cours de mécanique appliquée aux machines, deuxième section: Du joint brisé ou universel. Gauthiers-Villars 1836 et 1874. German trans.: Leske (1845, 1848) Lehrbuch der Anwendung der Mechanik auf Maschinen. Darmstadt
16. Roethlisberger J M, Aldrich F C (1967) The Tripot universal joint. SAE paper No. 690257
17. Graf v. Seherr-Thoss H-C, Schmelz F, Aucktor E (2002) Gelenke und Gelenkwellen 2nd ed. Springer, Berlin, Heidelberg, New York
18. Wittenburg J, Roberson R E (1982) Polhode and herpolhode cones in a generalized Hooke's joint. *ZAMM* 62:589–598